Computer Methods in Applied Mechanics and Engineering 452 (2026) 118721

Contents lists available at ScienceDirect

Comput. Methods Appl. Mech. Engrg.

journal homepage: www.elsevier.com/locate/cma

Optimal convergence of IgA collocation methods

Maria Roberta Belardo [a,*], Francesco Calabrò [b,a]

[a] Scuola Superiore Meridionale, Via Mezzocannone, 4, 80138, Napoli, Italy
[b] Dipartimento di Matematica e Applicazioni "Renato Caccioppoli", Università degli Studi di Napoli "Federico II", Complesso Universitario di Monte Sant'Angelo, Via Cintia, 80126, Napoli, Italy

ARTICLE INFO

Keywords:
Isogeometric analysis
Partial differential equations
Collocation methods

ABSTRACT

Isogeometric collocation discretizes the strong form of a PDE on smooth spline spaces and therefore avoids element integration, but its spatial accuracy is highly sensitive to the placement of the collocation nodes. For this reason methods are tested on linear elliptic problems in order to verify convergence properties. Classical choices such as Greville abscissae may yield suboptimal convergence in both H^1 and L^2 norms for several spline degrees and problem settings. Node sets derived from (estimated) superconvergent (Cauchy–Galerkin) points – e.g. alternating subsets, clustered variants, or least–squares sets – frequently improve the observed L^2 behaviour and in favourable cases approach the Galerkin benchmark, though this is not universal across all degrees, boundary conditions, and PDE types. In this paper we find for the first choices of points that recover optimal convergence for polynomial degrees $p = 4, 6, 8$. The construction is made in order to recover the symmetry inside every knot span also for even degrees, as done in the above mentioned methods. Although the exact reason for this behaviour could not be clearly identified, the numerical evidence suggests that restoring local symmetry recovers the optimal rate. Unfortunately, as most of the previously proposed methods, this results in a collocation system with more equations than degrees of freedom number of degrees of freedom, thus the overall system is solved in a least–square sense.

1. Introduction

Isogeometric analysis (IgA) [1] bridges computer-aided design (CAD) and numerical simulation by employing the same spline technologies (B-splines and NURBS) to represent geometry and approximate fields. Since its introduction, IgA has shown advantages over classical finite elements, including exact representation of common CAD geometries, higher inter-element smoothness, and a refined toolkit of *h*-, *p*-, and *k*-refinement strategies that enable high-order, high-regularity discretizations [2]. To reduce the complexity and implementation cost of isogeometric analysis, isogeometric collocation (IgA-C) has been investigated [3]. In Galerkin IgA, the discrete system is formed by integrating the PDE residual against a test space, which requires numerical quadrature and makes assembly expensive. Collocation, instead, enforces the strong form at a set of points, avoiding volume integrals and relying on point evaluations of spline basis functions and data. A reformulation in a variational context was also proposed by the same authors in Auricchio et al. [4], and detailed comparisons between isogeometric Galerkin and collocation methods have been made [5], however the theoretical system of the IgA-C method is yet to be firmly established. When the number of collocation points exceeds the degrees of freedom, the approach is commonly referred to as least–squares isogeometric collocation [6,7]. Convergence

* Corresponding author.
E-mail addresses: mariaroberta.belardo-ssm@unina.it (M.R. Belardo), calabro@unina.it (F. Calabrò).

https://doi.org/10.1016/j.cma.2025.118721
Received 10 October 2025; Received in revised form 28 November 2025; Accepted 29 December 2025
Available online 9 January 2026

and consistency results for IgA-C have been analyzed and established by Lin et al. [8,9], with analogous developments for least–squares collocation in Lin et al. [7]. A recent study further analyzes the spectral properties of least–squares IgA collocation, comparing the collocation and associated mass matrices with their Galerkin counterparts and showing that, under the same conditions, the growth of the operator-matrix condition number is slower than that of the Galerkin stiffness; therefore the linear systems of the least squares IgA-C method are better conditioned, particularly as the polynomial degree increases [10]. Isogeometric collocation has been applied in various fields, including contact and Neumann boundary conditions [11], explicit and implicit structural dynamics [12,13], fluid–structure interaction with immersed and hybrid formulations [14,15], cardiac electrophysiology [16], stabilized and structure-preserving formulations for fluid dynamics [17–19].

Efficiency and accuracy of IgA-C are greatly influenced by the selection of collocation points. Beyond Greville and Demko abscissae, several strategies select points informed by Galerkin superconvergence or variational arguments. In particular, the variational collocation framework [20] identifies Cauchy–Galerkin points whose exact use reproduces the Galerkin solution, and provides practical estimates of such sites. least–squares oversampling at superconvergent locations improves rates in specific settings [6], while determined schemes based on clustered selections of superconvergent points achieve optimal L^2 convergence for odd polynomial degrees [21]. For odd polynomial degrees the element–invariant superconvergent points proposed in literature exhibit a local symmetry inside every knot span: two abscissae are placed at equal distance from the element centre; these obtain optimal convergence. For even degrees the points used are the element boundaries and their midpoints; in these cases the convergence drops by one order. A different approach can be found in [22] where a Greville-based construction using basis transformations and recursive gradients establishes superconvergent collocation with a proof for odd degrees. Starting from these results, with the objective of restoring local symmetry inside every knot span, in this paper we explore the convergence of a least–square IgA-C. In particular, we develop for the first time a superconvergent collocation strategy for even-degree spline spaces.

The paper is organized as follows. We first fix notation and recall the spline spaces used in Section 2. In Section 3 we start with a description of collocation schemes, including the square and the least–square case, the inclusion of the boundary conditions, and appropriate choices of collocation points. In Section 4 we present the convergence results for random choices sets of collocation points with local symmetry and fix a choice of superconvergent collocation points. In Section 5 we detail numerical tests, both in one-dimensional and two-dimensional domains.

2. Notations on B-splines

The construction of a B-spline basis in one dimension requires two ingredients: the degree of the basis (denoted p) and a set of numbers called the knot vector. We restrict our analysis in $[0,1]$ and use the notation $\Xi = \{0 = \xi_1, \dots, \xi_{N+p+1} = 1\}$. The knots ξ_i are non-decreasing and denote the locations in parametric space where the parametrization can change, similar to element boundaries in standard FEA. The number N in the previous relation also represents the total number of functions in the basis. The basis functions themselves are defined through the Cox-de Boor recursion: the $p = 0$ basis functions are built as

$$B_{i,0}(x) = \begin{cases} 1 & \xi_i \le x \le \xi_{i+1} \\ 0 & \text{otherwise,} \end{cases} \tag{2.1}$$

for all $i = 1, \dots, N$, and higher-order basis functions are defined through

$$B_{i,j}(x) = \frac{\xi - \xi_i}{\xi_{i+j} - \xi_i} B_{i,j-1}(x) + \frac{\xi_{i+j+1} - \xi}{\xi_{i+j+1} - \xi_{i+1}} B_{i+1,j-1}(x). \tag{2.2}$$

for all polynomial degrees $j = 1, \dots, p$. Note that in the above relations, we set zero divided by zero is equal to zero. Let us introduce the vector of break points $\boldsymbol{\zeta} = \{\zeta_1, \dots, \zeta_{n_{el}}\}$ of knots without repetitions. For simplicity, we assume that all interior knots have a constant multiplicity r. This multiplicity determines the continuity of the basis at each break point: an interior knot repeated r times yields basis functions that are C^{p-r} continuous at that location. We denote by $q = p - r$ the uniform continuity order of the basis in the internal knots. If the first and last entries in the knot vector are repeated $p + 1$ times, the resulting spline basis interpolates the function at those endpoints. Such knot vectors, known as *open knot vectors*, facilitate the enforcement of the Dirichlet boundary condition, and this will always be the case of our treatment. With this notation, the one-dimensional B-spline space defined on the knot vector Ξ, polynomial degree p, and regularity q, is denoted as

$$S_q^p(\Xi) = \text{span}\{B_{i,p}\}_{i=1}^N. \tag{2.3}$$

The dimension N of a uniform spline space $S_q^p(\Xi)$ with interpolating end-conditions is easily computed as,

$$N := \#S_q^p(\Xi) = (p+1) + (n_{el} - 1)(p - q). \tag{2.4}$$

Note that in the maximum regularity case $q = p - 1$ this relation can be simplified in $N = p + n_{el}$. B-spline basis functions in higher dimensions are obtained by taking the tensor product of one-dimensional bases along each coordinate direction, allowing in principle for different polynomial degrees and knot vectors in each direction. Besides open knot vectors, we also consider *periodic* spline spaces, obtained by removing the end multiplicities and identifying degrees of freedom across the boundary. In 1D, with a uniform knot partition and maximum regularity, the periodic space is

$$S_{p,q}^{\text{per}}(\Xi) = \{\, v \in S_q^p(\Xi) \;:\; v(0) = v(1),\, v'(0) = v'(1), \dots, v^{(p-1)}(0) = v^{(p-1)}(1)\},$$

so that the basis functions and their derivatives up to order $q = p - 1$ coincide at the endpoints. For a mesh with n_{el} elements, this construction gives exactly n_{el} degrees of freedom in 1D. In this work we restrict ourselves to spline spaces with identical polynomial degrees and knot vectors in all directions, so that a single degree and a single knot vector fully define the space in any dimension.

3. Collocation of the strong form

The description of a collocation method starts from the strong form of a partial differential equation. Consider an open domain Ω with Lipschitz continuous boundary $\partial\Omega$, on which an unknown field variable u is defined. This variable is the solution to a partial differential equation and boundary conditions

$$\begin{cases} \text{Given } \mathcal{L},\ f,\ \mathcal{G}, \text{ and } g, \text{ find } u \text{ such that:} \\ \mathcal{L}u = f \quad \text{in } \Omega, \qquad \text{(a)} \\ \mathcal{G}u = g \quad \text{on } \partial\Omega. \qquad \text{(b)} \end{cases} \tag{3.1}$$

where $\mathcal{L}$ is the differential operator, f is a forcing term, $\mathcal{G}$ is the boundary operator, and g is the provided boundary data. Collocation methods approximate the solution to this problem with a linear combination of N basis functions $u^h(x) = \sum_{i=1}^{N} B_i(x)c_i$, where the superscript h denotes the dependence on a mesh size parameter, $\{B_i\}_{i=1}^{N}$ are the basis functions of a B-spline space of maximum continuity and $\{c_i\}_{i=1}^{N}$ are unknown coefficients of the sought numerical solution.

In order to solve the system in a least–squares collocation sense, we sample N_P points $\{x_\ell\}_{\ell=1}^{N_P}$ in the closure $\bar{\Omega}$, in general greater than the number of unknown coefficients of the numerical solution, namely, $N_P \geq N$. Just as in square collocation, these sampling points are also referred to as collocation points. We consider collocation sites both in the interior and, when boundary conditions are enforced by collocation, on the boundary, i.e., $x_\ell \in \Omega$ or $x_\ell \in \partial\Omega$. The full discrete system is formed by requiring the strong form of the PDE to hold at each of the collocation points, obtaining the following system

$$\begin{cases} \text{Given } \mathcal{L},\ f,\ \mathcal{G}, \text{ and } g, \text{ find } \underline{c} \in \mathbb{R}^N \text{ such that } u^h(x) = \sum_{i=1}^{N} B_i(x)c_i \text{ is solution of:} \\ \mathcal{L}\{u^h\}(x_\ell) = f(x_\ell) \quad \forall x_\ell \in \Omega, \qquad \text{(a)} \\ \mathcal{G}\{u^h\}(x_\ell) = g(x_\ell) \quad \forall x_\ell \in \partial\Omega. \qquad \text{(b)} \end{cases} \tag{3.2}$$

In the case of $N_P > N$, the approximate solution u^h is intended as the least–squares solution, determined by minimizing the sum of the squared residuals at these collocation points. When the differential operator is linear, arranging the unknowns of the numerical solution u^h into an $N \times 1$ vector, i.e., $\underline{c} = [c_1, c_2, \dots, c_N]^\top$, the system of Eq. (3.2) can be represented in matrix form by

$$\mathbb{L}\,\underline{c} = \underline{f}, \tag{3.3}$$

where $\mathbb{L} \in \mathbb{R}^{N_P \times N}$ collects the collocated evaluations of the governing operators acting on the basis functions at the sampling points x_ℓ, and $\underline{f} \in \mathbb{R}^{N_P}$ collects the corresponding right-hand side evaluations at the same sites. For interior points, the matrix entries involve evaluations of $\mathcal{L}\{B_i\}(x_\ell)$; the construction of the rows associated with the boundary operator $\mathcal{G}$ is discussed in the next paragraph. Notice that, because the number of equations is greater than the number of unknowns, in general the solution of the least–squares problem will not be exact on the collocation points, differing substantially from the square case. The mathematical foundation of this least–squares framework has been studied in [7], where the consistency and convergence properties are proved.

3.1. Imposition of boundary conditions

Boundary conditions in isogeometric collocation require different discrete treatments depending on their type. For Dirichlet boundaries, this is achieved by eliminating from the collocation system (3.3) the degrees of freedom associated with the prescribed boundary basis functions, and by inserting the corresponding coefficients induced by the boundary data. In this way, the collocation system is reduced to the unknown interior degrees of freedom while maintaining the exact satisfaction of the boundary values, also when the discrete system is solved in a least–squares sense. In the presence of periodic boundary conditions, we assemble the problem in a periodic spline space, so that periodicity of the field (and of its derivatives up to the basis continuity) is built into the approximation. Consequently, with suitably chosen collocation points periodically distributed on $[0, 1]$, both square and least–squares collocation enforce it exactly. Neumann boundary conditions are less direct to handle in collocation and require particular care. In the isogeometric framework, several strategies have been proposed in [11]. Similar alternatives are also discussed in the broader collocation and meshless least–squares literature; see [23,24]. However, enforcing Neumann data as hard constraints can deteriorate accuracy. In particular, for square collocation it has been shown that strong Neumann enforcement may lead to loss of accuracy in some situations [11]. Moreover, in least–squares superconvergent collocation, Anitescu et al. [6] report that imposing Neumann boundaries as exact constraints can reduce the convergence order. For these reasons, and with the aim of preserving optimal accuracy, we impose Neumann conditions by appending the corresponding boundary collocation equations to the global least–squares system. Specifically, on each Neumann edge we collocate the Neumann operator at boundary points and add these conditions to the least–squares system.

3.2. Choice of the collocation points

In the discussion of collocation methods so far, we have not yet defined appropriate collocation points for the spline bases, which affects the stability and order of accuracy of the method. We begin by defining the Greville abscissae (GP) associated with each

Table 1
Comparisons of orders of convergence for IgA-C with different choice of collocation points. Galerkin resolution is the reference method. Collocating the equation at Greville points reported as (C-GP); Least–Squares approximation at Superconvergent Points (LS-SP) from [6]; Collocation at Alternating Superconvergent Points (C-ASP) from [20]; Clustered Superconvergent Points (C-CSP) from [21].

	Galerkin	C-GP		LS-SP and C-CSP		C-ASP
		Odd p	Even p	Odd p	Even p	
L^2	$p+1$	$p-1$	p	$p+1$	p	p
H^1	p	$p-1$	p	p	p	p
H^2	$p-1$	$p-1$	$p-1$	$p-1$	$p-1$	$p-1$

Table 2
Superconvergent points for the second derivative on the reference element $[-1,1]$ (cf. [20]).

Degree	Second–derivative SP
$p=3$	$\pm\frac{1}{\sqrt{3}}$
$p=4$	$-1,\ 0,\ 1$
$p=5$	$\pm\frac{\sqrt{225-30\sqrt{30}}}{15}$
$p=6$	$-1,\ 0,\ 1$
$p=7$	± 0.504918567512

B-spline space using node averages as

$$\hat{\xi}_i = \frac{\xi_{i+1} + \ldots + \xi_{i+p}}{p}, \qquad i = 1, \ldots, N, \tag{3.4}$$

these are well known in the isogeometric literature for a number of properties, among which the fact that they typically give a stable interpolation. The use of the Greville abscissae of the numerical solution space is one of the most popular choice for square collocation, as they are simple to work with and give good quality results in practice. These are an approximation of the more stable Demko abscissae, which require an iterative algorithm to compute, and have the same order of convergence as the Greville abscissae. In the context of square collocation, this choice yields optimal error of accuracy in the H^2 norm for second-order problems under $h-$refinement, where h is the maximum length of elements, while converging to $\mathcal{O}(h^{p-1})$ or $\mathcal{O}(h^p)$ when the degree p is odd or even, respectively, in the L^2 and H^1 norms, see Table 1.

However, the optimal error for an isogeometric method is obtained with a Galerkin approximation, i.e. either $O(h^{p+1})$ or $O(h^p)$ for the L^2 and H^1 norm, respectively, regardless of the parity of p. To recover the Galerkin accuracy several alternatives reported as superconvergent have been proposed. Gomez and De Lorenzis [20] introduced the notion of *Cauchy-Galerkin points* (CG points), defined as the locations where the Galerkin residual vanishes, thus recovering optimal convergence. However, since they are not known a priori, the same authors estimate approximated Cauchy-Galerkin points under an element-invariance assumption, selecting the locations where the Galerkin second derivatives are provably superconvergent. They also described an alternating selection (C-ASP), obtained by taking one such superconvergent point per element, delivering uniform order p in the L^2 norm for both odd and even degrees. Under the same invariance assumption, Anitescu *et al.* [6] independently tabulated the same coordinates and employed all of them in a least–squares collocation framework, obtaining the LS–SP (*Least Square on Superconvergent Points*) method. This achieves optimal convergence in H^1 (and H^2) norm for all p, optimal L^2 for odd p, and one-order suboptimal L^2 for even p. Montardini *et al.* [21] later selected a locally symmetric subset of those nodes, termed *clustered superconvergent points* (C-CSP), and showed that a square collocation built on them recovers the optimal L^2 order for odd p. C-ASP, LS-SP, and C-CSP are thus all selected among the (approximated) superconvergent points listed in Table 2. Table 1 collects the convergence rates for the different collocation points and highlights their deviation from the Galerkin reference behaviour.

4. Symmetric superconvergent points for even degrees

Having introduced the basics of collocation methods, including basis functions and the definition of collocation points, we now focus on the case of even polynomial degrees. In this case, none of the element–invariant choices tabulated in [6,20] achieves superconvergence in the L^2 norm: for both $p=4$ and $p=6$, the abscissae lie at the element boundaries and at the midpoint, and the observed rate drops by one order. By contrast, for odd polynomial degrees the element–invariant superconvergent points display a local symmetry within each knot span, with two abscissae placed at equal distance from the element center. This was also noticed when using the same pattern inherited by the clustered set of C-CSP in [21] and was noticed to be crucial in order to attain the Galerkin order in the L^2 norm. Although the exact reason for this behaviour could not be clearly identified, the numerical evidence suggests that restoring local symmetry can recover the optimal rate.

Table 3
Mean L^2 and H^1 errors of u^h over one hundred random symmetric trials, together with the average convergence order computed from the reported values for polynomial degrees $p = 3 - 8$. This table refers to Problem 1, see Section 5.1.1. The values marked with an asterisk refer to the average of the first two refinements.

	Norm	$h = 1/8$	1/16	1/32	1/64	avg. order
$p = 3$	$\|u - u^h\|_{L^2}$	1.61×10^{-3}	3.95×10^{-4}	9.96×10^{-5}	2.56×10^{-5}	
	order	–	2.03	1.99	1.96	1.99
	$\|u - u^h\|_{H^1}$	5.25×10^{-3}	1.25×10^{-3}	3.13×10^{-4}	8.05×10^{-5}	
	order	–	2.07	1.99	1.96	2.01
$p = 4$	$\|u - u^h\|_{L^2}$	3.53×10^{-4}	1.18×10^{-5}	3.52×10^{-7}	1.23×10^{-8}	
	order	–	4.91	5.06	4.84	4.94
	$\|u - u^h\|_{H^1}$	2.50×10^{-3}	1.17×10^{-4}	5.01×10^{-6}	2.25×10^{-7}	
	order	–	4.42	4.54	4.48	4.48
$p = 5$	$\|u - u^h\|_{L^2}$	5.82×10^{-5}	6.73×10^{-7}	2.62×10^{-8}	1.53×10^{-9}	
	order	–	6.43	4.68	4.10	5.07
	$\|u - u^h\|_{H^1}$	4.22×10^{-4}	5.20×10^{-6}	1.06×10^{-7}	4.91×10^{-9}	
	order	–	6.34	5.62	4.43	5.46
$p = 6$	$\|u - u^h\|_{L^2}$	1.64×10^{-4}	1.70×10^{-6}	1.50×10^{-8}	1.25×10^{-10}	
	order	–	6.59	6.82	6.91	6.77
	$\|u - u^h\|_{H^1}$	1.24×10^{-3}	1.80×10^{-5}	2.24×10^{-7}	2.62×10^{-9}	
	order	–	6.11	6.33	6.42	6.29
$p = 7$	$\|u - u^h\|_{L^2}$	9.90×10^{-5}	1.97×10^{-7}	4.31×10^{-10}	1.98×10^{-12}	
	order	–	8.97	8.84	7.76	8.53
	$\|u - u^h\|_{H^1}$	7.94×10^{-4}	2.21×10^{-6}	6.78×10^{-9}	5.32×10^{-11}	
	order	–	8.49	8.35	6.99	7.94
$p = 8$	$\|u - u^h\|_{L^2}$	8.13×10^{-9}	1.94×10^{-11}	5.23×10^{-14}	8.48×10^{-14}	
	order	–	8.70	8.53	-0.69	8.62*
	$\|u - u^h\|_{H^1}$	1.13×10^{-7}	3.34×10^{-10}	9.38×10^{-13}	1.64×10^{-13}	
	order	–	8.40	8.47	2.51	8.44*

To further investigate this relation, we carried out numerical experiments in which, for each degree $p = 3, \dots, 8$, one hundred random symmetric perturbations of the interior abscissae were generated within every knot span, and the differential problems were then solved with the least–squares collocation method. Tables 3–5 correspond to the one-dimensional Dirichlet test problems from Section 5. Within each table, the reported results refer to the averages of errors over all trials. For all three problems, the case $p = 3$ exhibits an essentially second-order convergence in both norms, and therefore does not display any visible gain nor the superconvergence. In contrast, from $p = 4$ onwards the symmetric configuration of collocation points favors a convergence rate higher than the Greville standard. In the L^2 norm we observe rates close to, and often slightly above, the superconvergent rate $p + 1$, while the H^1 errors converge with rates close to order p, or slightly above. This enhancement is particularly evident for $p = 6$ and $p = 7$, where the L^2 error decays with slopes around $p + 1$ (or higher) across all three test problems. In particular, for even degrees such as $p = 4$ and $p = 6$, the locally symmetric random patterns achieve a genuinely superconvergent decay in the L^2 norm, whereas such a behaviour had not been observed for any of the collocation points previously examined. The results for $p = 8$ follow the same trend on the first refinement levels, with observed rates in L^2 and H^1 again close to $p + 1$ and p, respectively. On the finest meshes, however, the errors approach the limit of double-precision accuracy, and the convergence reaches a plateau that affects the reported convergence order. However, it is unclear why the polynomial case $p = 3$ does not benefit from the symmetrical arrangement of the collocation points. As assumed in [21], it could be that the superconvergence is due to some error cancellation resulting from the local symmetry of the point distribution. Since the second derivatives of cubic splines are piecewise constant polynomials, they may not benefit from this arrangement except at points where the second derivative is superconvergent with respect to the Galerkin solution.

Motivated by the foregoing evidence, and in order to fix a systematic choice applicable in all subsequent simulations, we impose, for $p \in \{4, 6, 8\}$, a new symmetric interior pattern, prescribing two abscissae $\xi^* = 0.5 \pm \delta_p$ with $\delta_p \in (0, 0.5)$. Then, the optimal value of δ_p is determined by a refinement search: starting from a coarse grid on δ_p we repeatedly refined the search in the region where the order of the error evaluated in the L^2 norm of the non-homogeneous Dirichlet Poisson problem of Section 5.1.1 was highest; the smallest refinement step used in the process was 10^{-7}. Table 6 lists the best symmetric pairs obtained for $p = 4, 6, 8$, together with the average convergence order computed over uniform mesh refinements from $n_{el} = 8$ to $n_{el} = 32$ for the Dirichlet one-dimensional test problems of Section 5. Using these symmetric abscissae, least–squares collocation achieves the optimal convergence for even degrees, matching the performance obtained for odd degrees with LS-SP or C-CSP. Fig. 1 contrasts the previously used second-derivative superconvergent set with the proposed even-degree configuration: the new distribution places symmetric interior nodes within each knot element and also includes the endpoints $x = 0$ and $x = 1$ so that Dirichlet boundary conditions are imposed exactly.

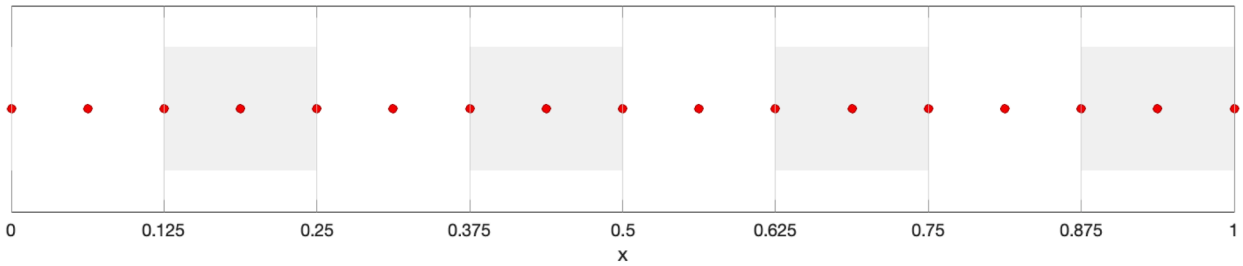

(a) $p = 4$, $n_{el} = 8$

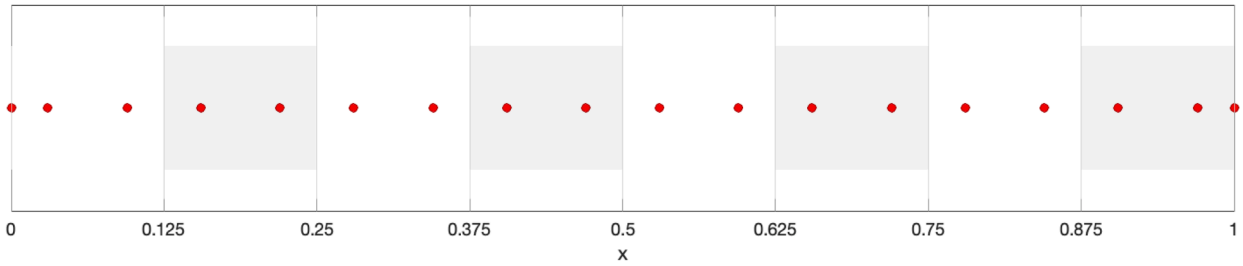

(b) $p = 4$, $n_{el} = 8$

Fig. 1. Distribution of Second Derivative SP points tabulated in Table 2 (top), and the new proposed superconvergent points for even degrees (bottom) tabulated in Table 6.

Table 4
Mean L^2 and H^1 errors of u^h over one hundred random symmetric trials, together with the average convergence order computed from the reported values for polynomial degrees $p = 3 - 8$. This table refers to Problem 2, see Section 5.1.2. The values marked with an asterisk refer to the average of the first two refinements.

	Norm	$h = 1/8$	1/16	1/32	1/64	avg. order
$p = 3$	$\|u - u^h\|_{L^2}$	1.99×10^{-3}	4.67×10^{-4}	1.21×10^{-4}	2.99×10^{-5}	
	order	–	2.09	1.95	2.01	2.02
	$\|u - u^h\|_{H^1}$	7.78×10^{-3}	1.77×10^{-3}	4.53×10^{-4}	1.11×10^{-4}	
	order	–	2.13	1.97	2.02	2.04
$p = 4$	$\|u - u^h\|_{L^2}$	2.48×10^{-4}	4.27×10^{-6}	6.80×10^{-8}	2.36×10^{-9}	
	order	–	5.86	5.97	4.85	5.56
	$\|u - u^h\|_{H^1}$	2.56×10^{-3}	5.98×10^{-5}	1.27×10^{-6}	3.85×10^{-8}	
	order	–	5.42	5.55	5.05	5.34
$p = 5$	$\|u - u^h\|_{L^2}$	1.21×10^{-4}	1.01×10^{-6}	1.53×10^{-8}	7.70×10^{-10}	
	order	–	6.90	6.05	4.31	5.75
	$\|u - u^h\|_{H^1}$	9.36×10^{-4}	9.88×10^{-6}	1.26×10^{-7}	4.74×10^{-9}	
	order	–	6.57	6.30	4.73	5.86
$p = 6$	$\|u - u^h\|_{L^2}$	4.44×10^{-4}	3.26×10^{-6}	2.60×10^{-8}	1.91×10^{-10}	
	order	–	7.09	6.97	7.09	7.05
	$\|u - u^h\|_{H^1}$	4.04×10^{-3}	3.56×10^{-5}	3.82×10^{-7}	3.89×10^{-9}	
	order	–	6.83	6.54	6.62	6.66
$p = 7$	$\|u - u^h\|_{L^2}$	2.72×10^{-4}	6.88×10^{-7}	1.18×10^{-9}	4.10×10^{-12}	
	order	–	8.63	9.18	8.17	8.66
	$\|u - u^h\|_{H^1}$	2.08×10^{-3}	7.39×10^{-6}	1.78×10^{-8}	1.02×10^{-10}	
	order	–	8.14	8.70	7.45	8.10
$p = 8$	$\|u - u^h\|_{L^2}$	1.33×10^{-8}	3.18×10^{-11}	8.14×10^{-14}	9.47×10^{-14}	
	order	–	8.70	8.61	0.21	8.65*
	$\|u - u^h\|_{H^1}$	1.15×10^{-7}	3.40×10^{-10}	9.58×10^{-13}	1.62×10^{-13}	
	order	–	8.40	8.47	2.56	8.43*

Table 5
Mean L^2 and H^1 errors of u^h over one hundred random symmetric trials, together with the average convergence order computed from the reported values for polynomial degrees $p = 3 - 8$. This table refers to Problem 3, see Section 5.1.3. The values marked with an asterisk refer to the average of the first two refinements.

p	Norm	$h = 1/8$	1/16	1/32	1/64	avg. order
$p = 3$	$\|u - u^h\|_{L^2}$	5.16×10^{-3}	1.23×10^{-3}	3.12×10^{-4}	6.73×10^{-5}	
	order	–	2.07	1.98	2.21	2.09
	$\|u - u^h\|_{H^1}$	2.69×10^{-2}	6.26×10^{-3}	1.58×10^{-3}	3.40×10^{-4}	
	order	–	2.10	1.99	2.22	2.10
$p = 4$	$\|u - u^h\|_{L^2}$	1.91×10^{-3}	5.82×10^{-5}	1.91×10^{-6}	6.68×10^{-8}	
	order	–	5.04	4.93	4.84	4.94
	$\|u - u^h\|_{H^1}$	1.64×10^{-2}	6.70×10^{-4}	2.88×10^{-5}	1.24×10^{-6}	
	order	–	4.61	4.54	4.54	4.56
$p = 5$	$\|u - u^h\|_{L^2}$	7.16×10^{-4}	6.74×10^{-6}	1.93×10^{-7}	1.13×10^{-8}	
	order	–	6.73	5.12	4.10	5.32
	$\|u - u^h\|_{H^1}$	6.29×10^{-3}	6.93×10^{-5}	1.21×10^{-6}	5.78×10^{-8}	
	order	–	6.50	5.84	4.39	5.58
$p = 6$	$\|u - u^h\|_{L^2}$	2.71×10^{-3}	1.97×10^{-5}	1.59×10^{-7}	1.42×10^{-9}	
	order	–	7.10	6.95	6.81	6.96
	$\|u - u^h\|_{H^1}$	2.44×10^{-2}	2.42×10^{-4}	2.60×10^{-6}	3.12×10^{-8}	
	order	–	6.66	6.54	6.38	6.53
$p = 7$	$\|u - u^h\|_{L^2}$	3.84×10^{-3}	5.14×10^{-6}	1.13×10^{-8}	2.06×10^{-11}	
	order	–	9.55	8.83	9.10	9.16
	$\|u - u^h\|_{H^1}$	3.64×10^{-2}	6.69×10^{-5}	1.95×10^{-7}	4.83×10^{-10}	
	order	–	9.09	8.42	8.66	8.72
$p = 8$	$\|u - u^h\|_{L^2}$	1.16×10^{-7}	2.35×10^{-10}	5.78×10^{-13}	1.04×10^{-14}	
	order	–	8.94	8.67	5.79	8.80*
	$\|u - u^h\|_{H^1}$	1.49×10^{-6}	3.56×10^{-9}	9.56×10^{-12}	7.47×10^{-14}	
	order	–	8.70	8.54	6.99	8.62*

Table 6
Superconvergent points ξ^* found numerically on the reference element $[-1, 1]$, and the L^2 order of convergence attained for the Dirichlet one-dimensional problem of Section 5.1.

Degree	ξ^*	Problem 1	Problem 2	Problem 3
$p = 4$	± 0.519141429	5.2207	5.0306	5.2649
$p = 6$	± 0.506247316	6.8997	7.0087	6.9092
$p = 8$	± 0.508216116	9.2652	8.8675	8.9874

Table 7
Unified element–invariant superconvergent points for LS collocation (odd degrees from [6], even degrees proposed here).

Degree	Superconvergent LS points
$p = 3$	$\pm \frac{1}{\sqrt{3}}$
$p = 4$	± 0.519141429
$p = 5$	$\pm \frac{\sqrt{225 - 30\sqrt{30}}}{15}$
$p = 6$	± 0.506247316
$p = 7$	± 0.504918567512
$p = 8$	± 0.508216116

5. Numerical results

We now present numerical results for the proposed least–squares collocation scheme with the new symmetric abscissae for even degrees and the tabulated superconvergent points for the odd cases (see Table 2 and Table 6). The method is first tested on four one-dimensional benchmark problems (with Dirichlet and periodic boundary conditions) to verify the L^2 and H^1 errors and their convergence orders. We then consider three two-dimensional examples, two on the unit square and one on a mapped domain, where

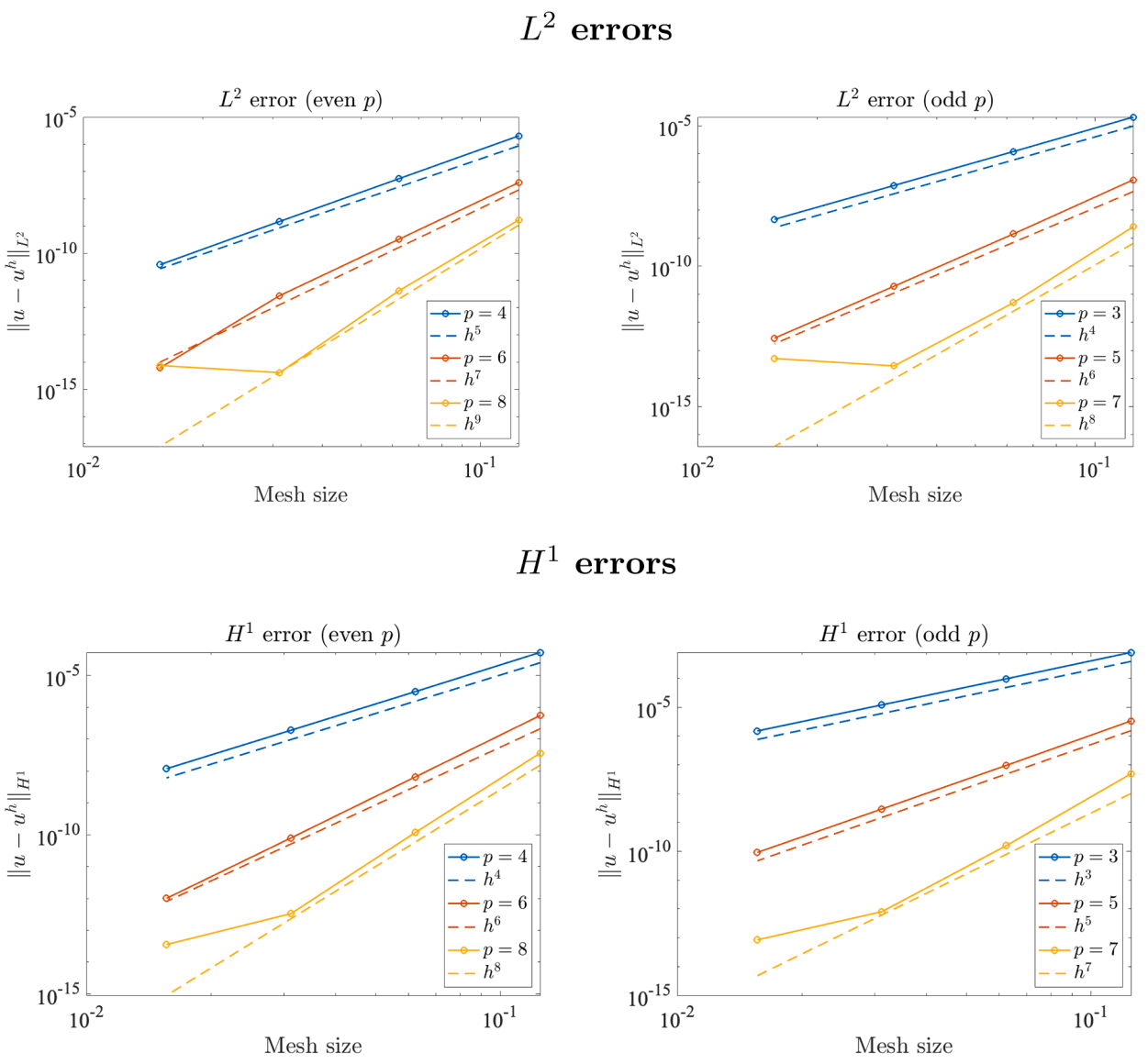

Fig. 2. L^2 and H^1 error plots for the one-dimensional elliptic problem in $[0, 1]$, namely Problem 1 of Section 5.1.1.

the same quantities are evaluated. In all presented tests of this section we observe order $p + 1$ for the error measured in L^2 norm, and order p for the error measured in H^1 norm for the proposed collocation points, equaling the optimal convergence rate of the Galerkin case. In all numerical experiments, the overdetermined collocation systems are solved in MATLAB using the backslash operator.

5.1. One-dimensional problems

We present our results and test our formulation considering a 1D linear second-order differential equation with a unique smooth solution in the following form:

$$-u'' + a_1 u' + a_0 u = f \text{ in } [0, 1], \tag{5.1}$$

$$u(0) = \alpha, u(1) = \beta, \tag{5.2}$$

where a_0, a_1, $f : [0, 1] \to \mathbb{R}$ are sufficiently regular functions, and α, $\beta \in \mathbb{R}$ are given boundary values. The choices of the coefficients are detailed in the subsequent sections.

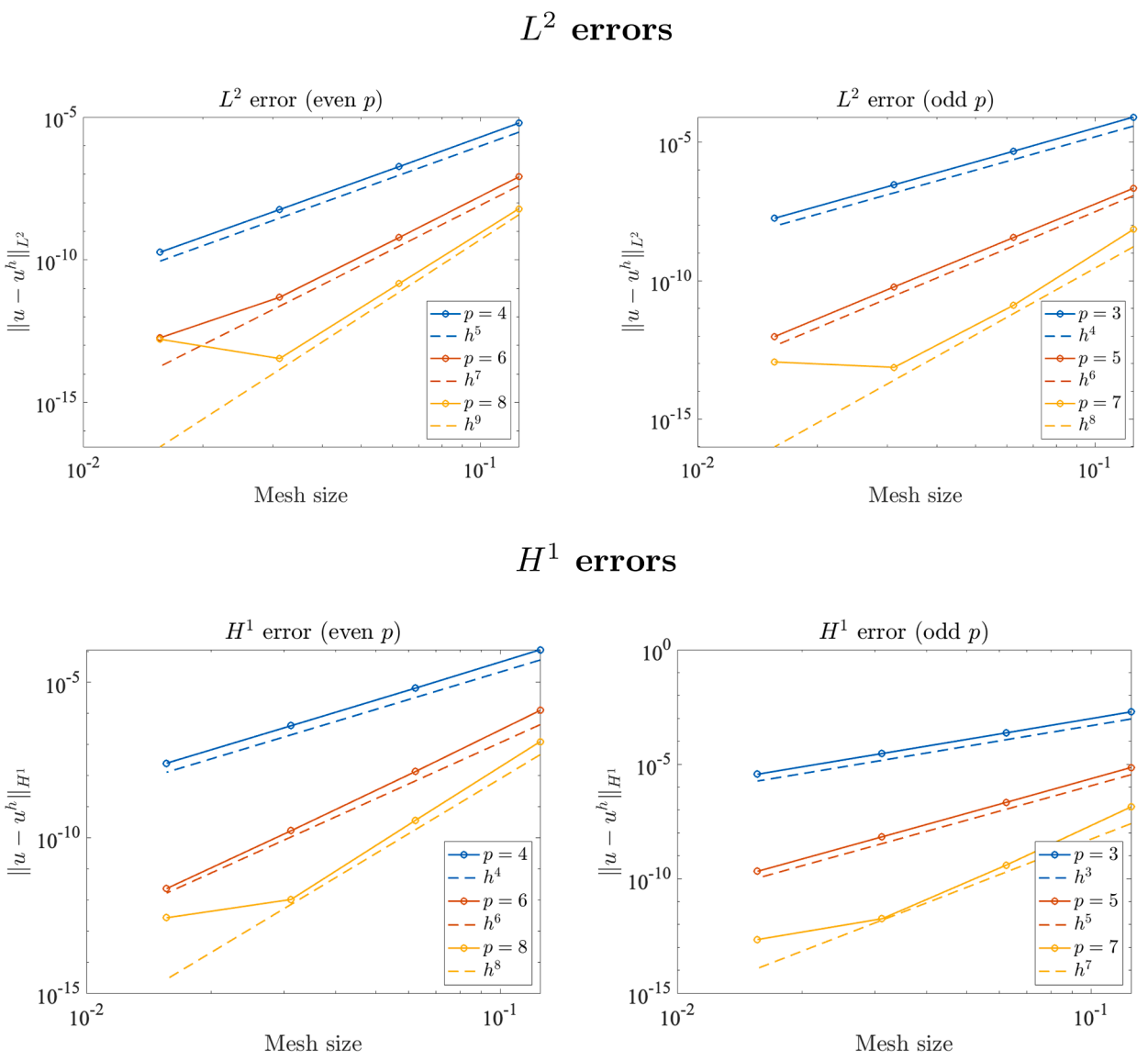

Fig. 3. L^2 and H^1 error plots for the one-dimensional reaction–advection–diffusion problem in $[0, 1]$, namely Problem 2 of Section 5.1.2.

5.1.1. Problem 1

We begin by testing the method with a Poisson problem, with coefficients $a_1 = 0$, $a_0 = 0$, $f(x) = \pi^2 \sin(\pi x)$ in the problem (5.1), homogeneous Dirichlet boundary conditions, whose exact solution is $u(x) = \sin(\pi x)$. As previously discussed, this is the test we use to find the element–invariant configuration with internal symmetry that provides the best convergence order. The detailed results are shown in Fig. 2, confirming what was reported at the beginning of this Section.

5.1.2. Problem 2

In the second problem we also verify the influence of the differential operator, by considering nonzero a_0 and non constant a_1 in the Dirichlet Problem (5.1). In detail, we consider $a_1(x) = x$, $a_0 = 1$ and $f(x) = x(e^x \sin(\pi x) + \pi e^x \cos(\pi x)) - 2\pi e^x \cos(\pi x) + \pi^2 e^x \sin(\pi x)$, whose exact solution is $u(x) = \sin(\pi x)e^x$. Fig. 3 reports the obtained results that confirm what was noticed previously.

5.1.3. Problem 3

In this test we further probe the role of the differential operator under non-homogeneous Dirichlet boundary conditions. We consider the reaction–advection–diffusion case, with coefficients $a_1(x) = x$, $a_0 = (1 + x^2)$ and $f(x) = \left(\frac{9\pi^2}{4} + 1 + x^2\right) \sin\left(\frac{3\pi}{2} x\right) - \frac{3\pi}{2} x \cos\left(\frac{3\pi}{2} x\right)$, with prescribed exact solution $u(x) = -\sin\left(\frac{3\pi}{2} x\right)$ and boundary data $u(0) = 0$ and $u(1) = 1$. The results in Fig. 4 exhibit the same behaviour observed in Problems 5.1.1–5.1.2, matching the expected optimal rates.

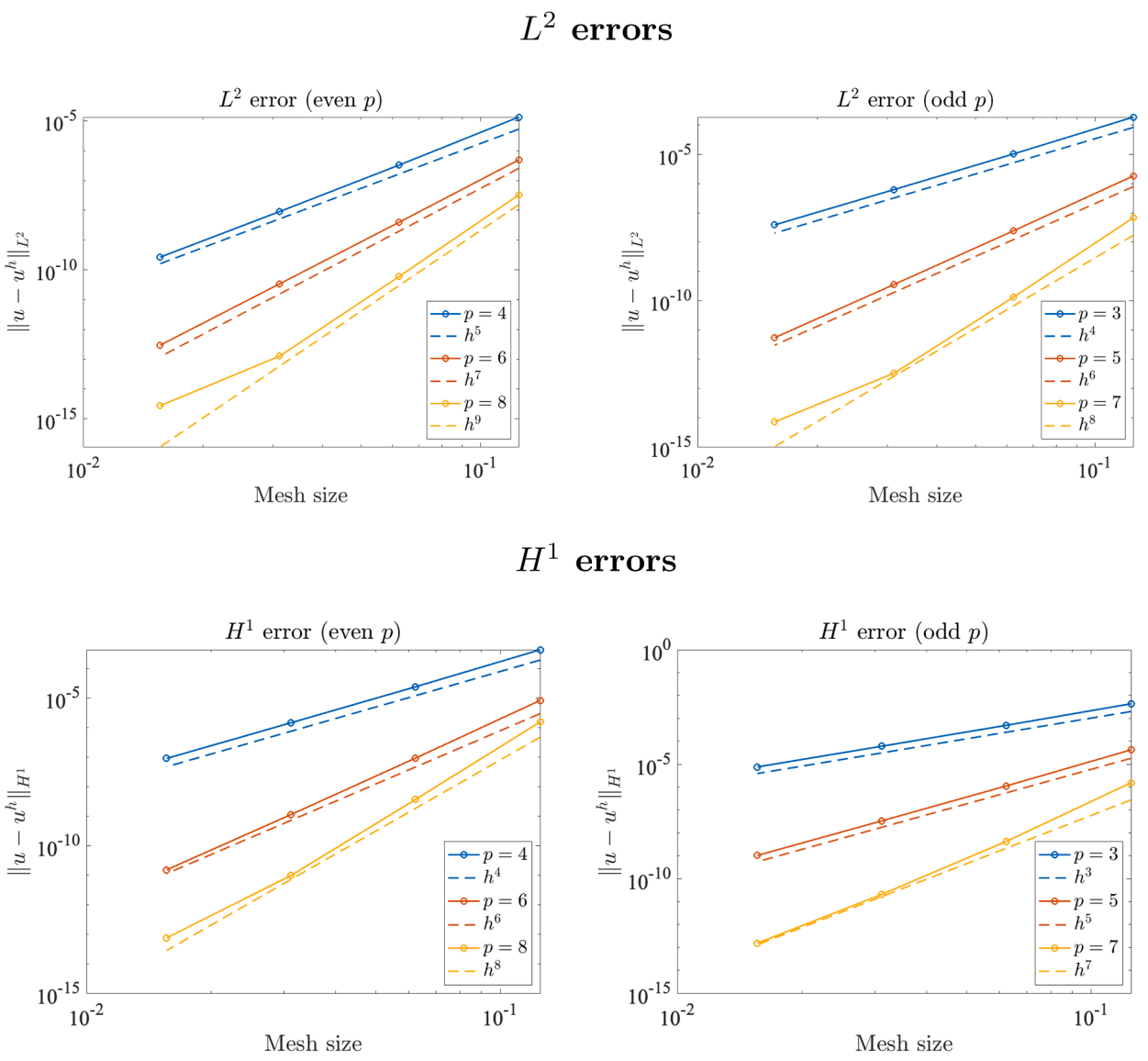

Fig. 4. L^2 and H^1 error plots for the one-dimensional reaction–advection–diffusion problem in $[0, 1]$, namely Problem 3 of Section 5.1.3.

5.1.4. Problem 1P

We consider a periodic problem in the form of (5.1), with boundary conditions $u(0) = u(1)$ and $u'(0) = u'(1)$. We set $a_0 = 1$, $a_1 = 1$ and prescribe the exact solution $u(x) = \sin(2\pi x)$, which yields $f(x) = (1 + 4\pi^2)\sin(2\pi x) + 2\pi\cos(2\pi x)$. The discretization employs the periodic counterpart of the maximum–regularity B-spline space. The collocation abscissae follow exactly the same per–element pattern as in the Dirichlet tests, which is already compatible with periodicity. We also use this solution to examine the sensitivity of the proposed collocation points to non-equispaced knot vectors. In particular, for each mesh of the convergence analysis, we perform random perturbations to the elements of an equispaced knot vector, replacing each internal knot ξ_i by $\hat{\xi}_i = \xi_i + \frac{1}{10n_{el}} X_i$, with X_i independent random distributions with range in $[-1, 1]$. The corresponding results in Fig. 5 show that the L^2 error is more sensitive than the H^1 error to such perturbations: interestingly, odd degrees appear more affected by the random perturbations than even degrees, which display a noticeably more robust behaviour and the asymptotic rate $p + 1$ is essentially preserved. In contrast, the H^1 error consistently follows the expected order p across all degrees.

5.2. Two-dimensional problems

The least–squares collocation with the proposed collocation points is now tested on two-dimensional boundary value problems of Poisson type,

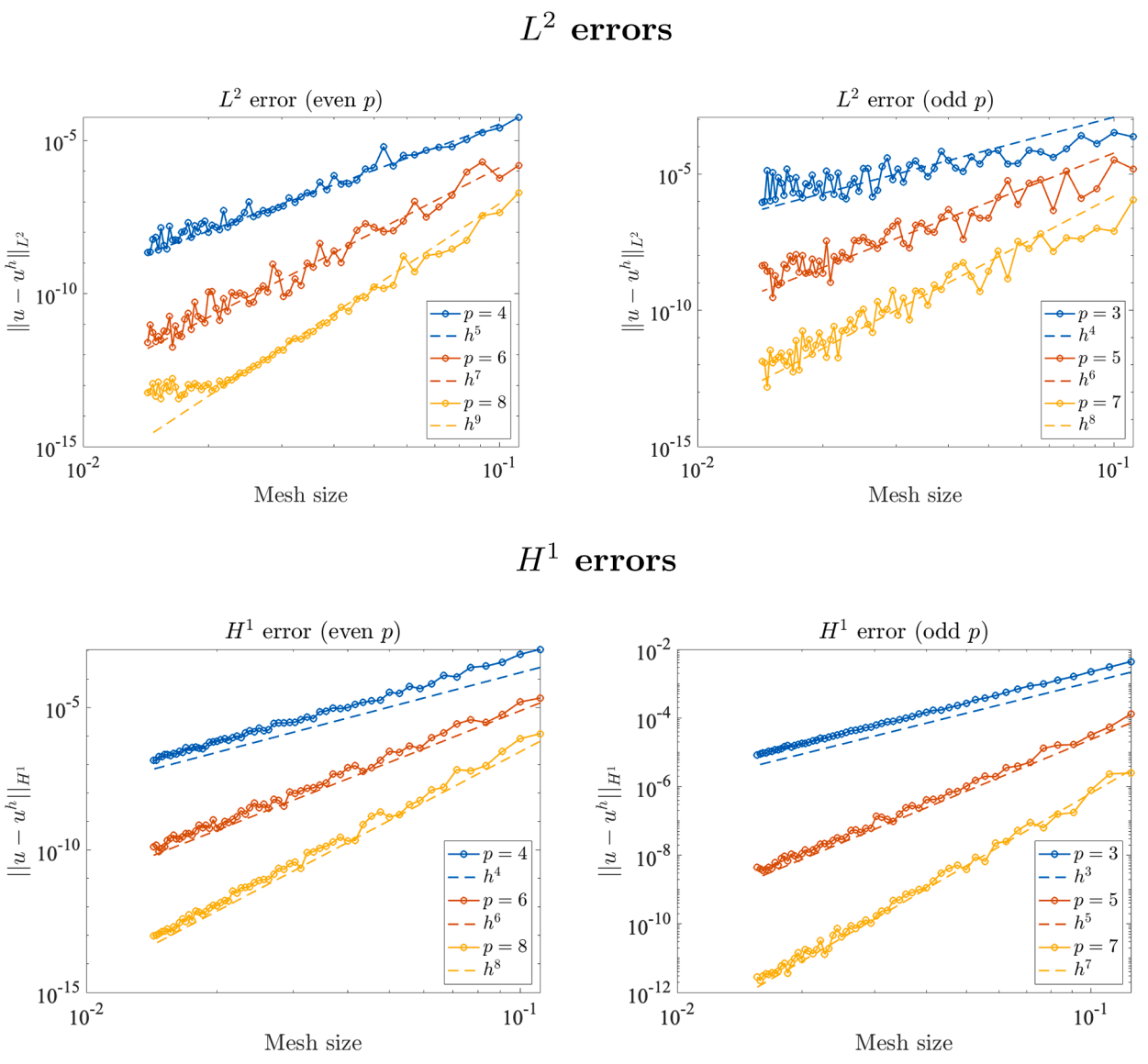

Fig. 5. L^2 and H^1 error plots for the one-dimensional periodic problem of Section 5.1.4.

$$-\Delta u = f \quad \text{in } \Omega, \tag{5.3}$$

$$u = g_D \quad \text{on } \Gamma_D, \tag{5.4}$$

$$\nabla u \cdot \mathbf{n} = g_N \quad \text{on } \Gamma_N, \tag{5.5}$$

where $\partial\Omega = \Gamma_D \cup \Gamma_N$ and $\Gamma_D \cap \Gamma_N = \emptyset$. Again we test in cases where the solution is known. We use two-dimensional collocation grids obtained by tensorization of the one-dimensional abscissae from Section 5.1, and, when needed, map the same parametric nodes to curved geometries. Fig. 6 illustrates the collocation points on the unit square and on a quarter annulus.

5.2.1. Problem 4

We consider $\Omega = [0,1]^2$ with exact solution $u(x,y) = \sin(\pi x)\sin(\pi y)$, thus $f(x,y) = 2\pi^2 \sin(\pi x)\sin(\pi y)$ and homogeneous Dirichlet boundary conditions. The discretization uses tensor–product B–splines on the open uniform knot vectors described in Section 2; collocation nodes are obtained by tensorizing the one–dimensional abscissae on $[0,1]^2$ (see also Fig. 6). The resulting L^2 and H^1 errors under h–refinement are reported in Fig. 7, confirming the expected convergence rates (L^2 : p+1, H^1 : p) for all polynomial degrees considered.

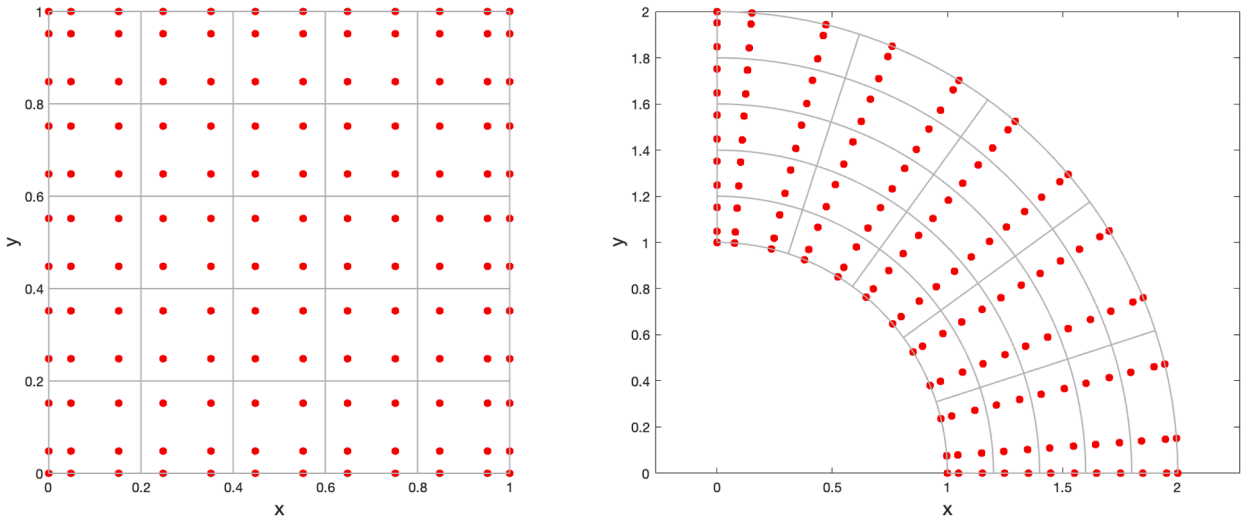

Fig. 6. Tensor-product collocation points generated by the even-degree LS superconvergent points. Left: square domain $[0,1]^2$ with the knot-element grid. Right: quarter annulus $r \in [1,2]$, $\theta \in [0,\pi/2]$ obtained by polar mapping of the same one-dimensional abscissae. Endpoints are included to enable exact imposition of Dirichlet boundary conditions. .

5.2.2. Problem 5

We next consider a curved domain given by a quarter annulus with inner and outer radii $r_{in} = 1$ and $r_{out} = 2$. The discretization is built in the parametric space $Q = [0,1]^2$ with tensor–product B–splines as in the square case, while the physical geometry Ω is described by the smooth bijective map $\Phi : Q \to \Omega$

$$\Phi(\xi,\eta) = \big((1+\xi)\cos(\tfrac{\pi}{2}\eta),\ (1+\xi)\sin(\tfrac{\pi}{2}\eta)\big), \qquad (\xi,\eta) \in Q.$$

Collocation points are selected in the parametric domain and evaluated in the physical domain via Φ. Basis functions of the discretization are the pull–backs of the parametric B–splines, and the differential operators are computed by the standard pull–back through $D\Phi$. We prescribe the exact solution $u(x,y) = -(x^2+y^2-1)(x^2+y^2-4)\,x\,y^2$, which vanishes on $\partial\Omega$, whose corresponding right–hand side is $f(x,y) = 2\,x\Big(x^4 + 22x^2y^2 - 5x^2 + 21y^4 - 45y^2 + 4\Big)$. Fig. 8 reports the errors, the observed orders of convergence are as expected: optimal order in L^2 and H^1 norms.

5.2.3. Problem 6

We consider a Poisson problem in $\Omega = [0,1]^2$ with mixed Dirichlet–Neumann boundary conditions, and manufactured solution $u(x,y) = \sin(\pi x)\sin(\pi y)\,e^{x+y}$. We prescribe homogeneous Dirichlet data on three sides, $u = 0$ on $\{0,1\}\times[0,1] \cup [0,1]\times\{0\}$, and a Neumann condition on the top edge, $\partial_y u(x,1) = g_N(x)$ with $g_N(x) = -\pi e^{x+1}\sin(\pi x)$ for $x \in (0,1)$. Dirichlet boundaries are enforced by eliminating the corresponding boundary degrees of freedom. On the Neumann edge $y = 1$, we collocate the flux equation $\partial_y u = g_N$ at Greville abscissae along the boundary, and solve them with the global least–squares system. Fig. 9 reports the L^2 and H^1 errors under h–refinement. The results confirm the optimal H^1 convergence and show that the proposed points preserve an enhanced L^2 behaviour also with mixed boundary conditions.

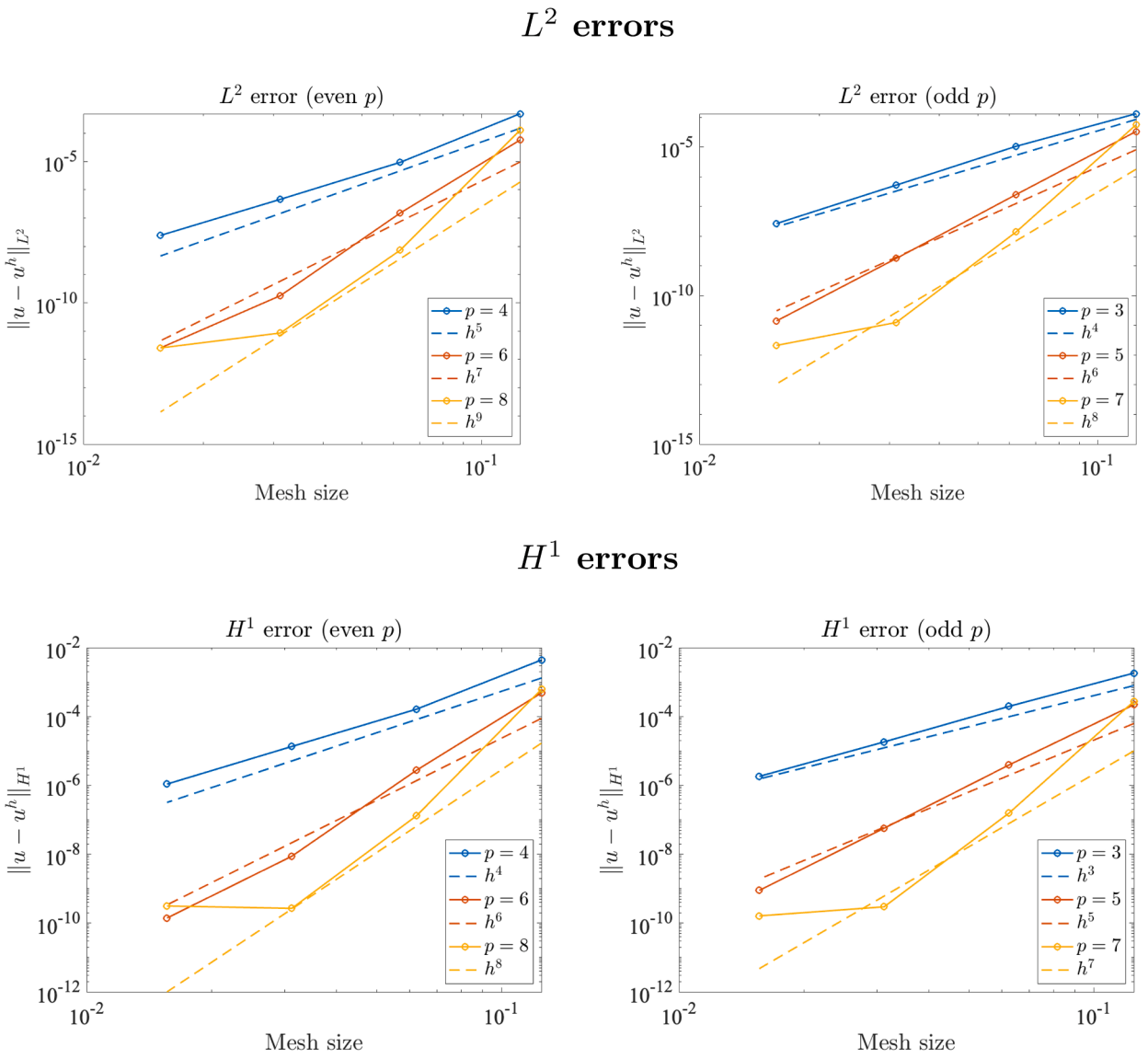

Fig. 7. L^2 and H^1 error plots for the 2D Poisson problem in $[0, 1]^2$, namely Problem 4 of Section 5.2.1.

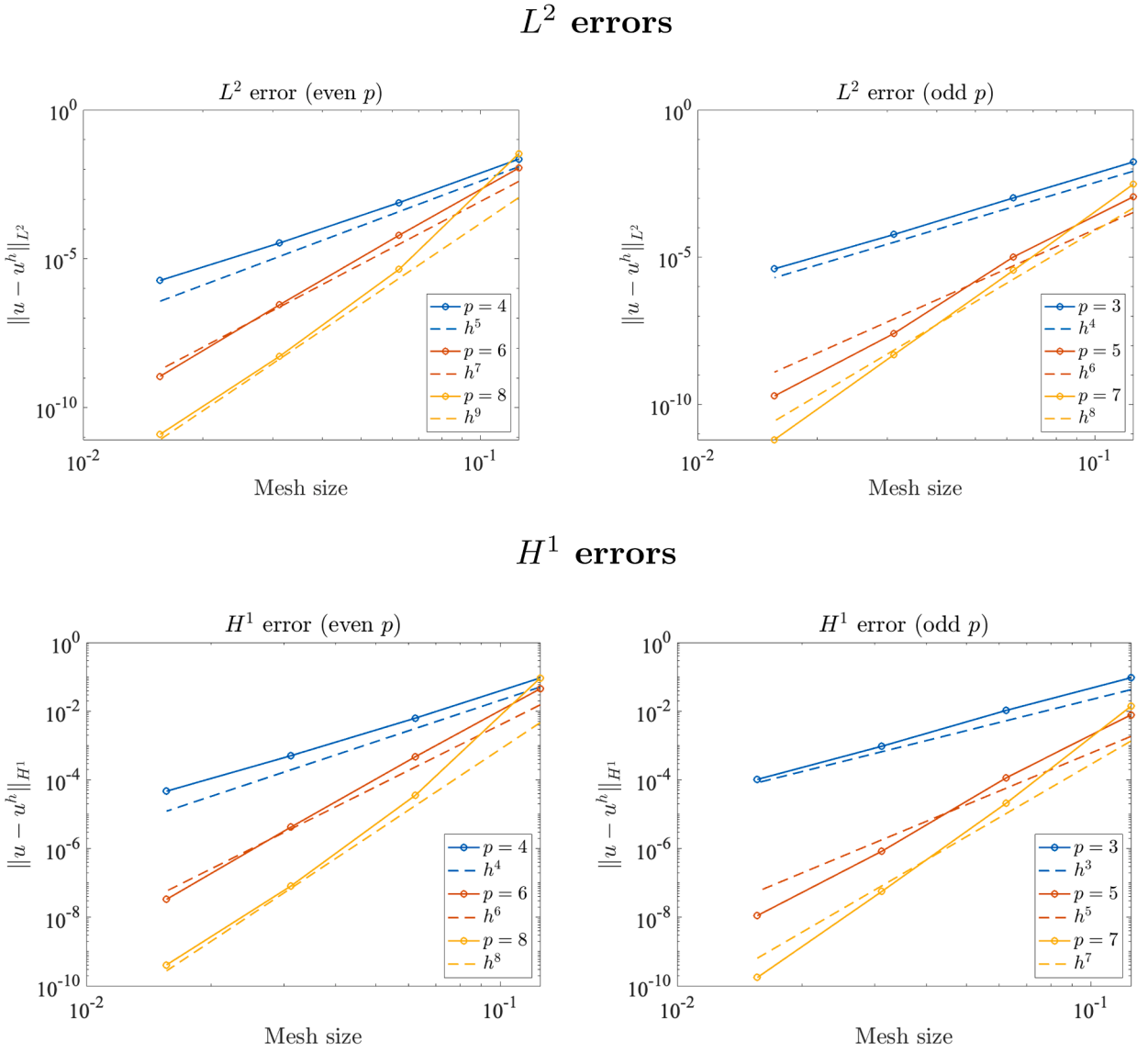

Fig. 8. L^2 and H^1 error plots for the 2D Poisson problem in the quarter annulus, namely Problem 5 of Section 5.2.2.

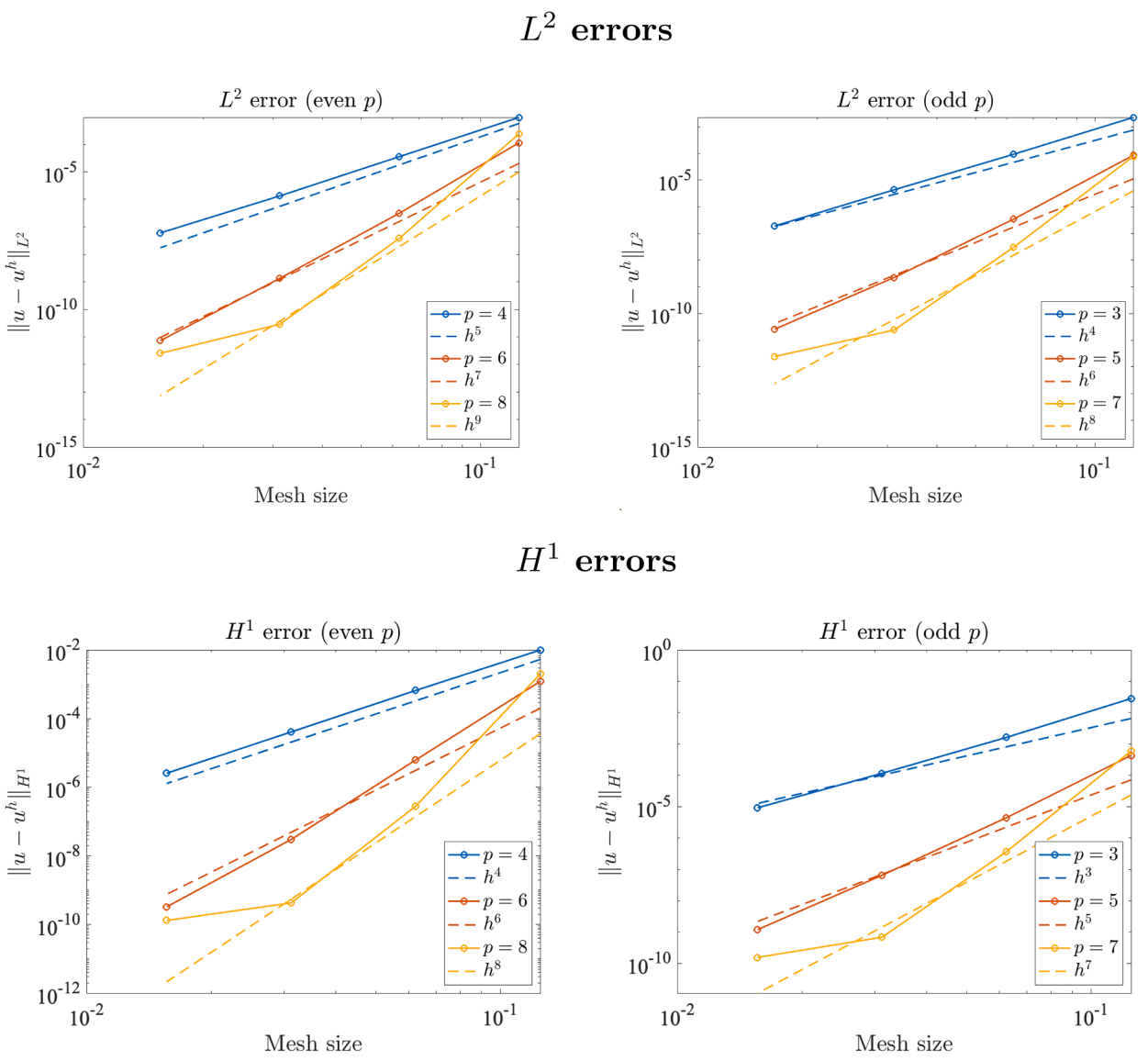

Fig. 9. L^2 and H^1 error plots for the 2D Poisson problem with mixed boundary conditions, namely Problem 6 of Section 5.2.3.

6. Conclusions

In the present paper we have considered the choice of collocation points in the IgA setting, that recover the same order of convergence of the Galerkin case, that is usually referred to as optimal. In the literature, we found such optimal choices for odd degrees, while even polynomial degrees always led to some suboptimality. By carrying out extensive simulations, we propose a new choice of points for the cases $p = 4, 6, 8$ that match optimal convergence. A unified summary of the recommended abscissae is reported in Table 7, combining the known odd–degree choices with the even–degree ones identified here. We point out that in the odd cases, by alternating points, authors in [21] were able to find a set of points that not only give superconvergence, but also squares the final collocation system; in our case we obtain superconvergence in the least–squares setting. Furthermore, our experiments in Tables 3–5 show that local symmetry systematically favors superconvergence for higher polynomial degrees ($p \geq 4$), suggesting that the proposed abscissae need not be unique and that alternative symmetric interior patterns may achieve comparable accuracy. In addition to matching the convergence orders achieved by odd–degree LS–SP points in the framework of [6], the even–degree abscissae proposed here yield comparable error magnitudes in both L^2 and H^1 norms across the tested meshes. Test examples give high accuracy with modest computational cost and do not suffer from reduced convergence related to the least–square resolution.

CRediT authorship contribution statement

Maria Roberta Belardo: Writing – review & editing, Writing – original draft, Software, Methodology, Investigation, Formal analysis, Conceptualization; **Francesco Calabrò:** Writing – review & editing, Writing – original draft, Conceptualization.

Data availability

No data was used for the research described in the article.

Declaration of competing interest

The authors declare that they have no known competing financial interests or personal relationships that could have appeared to influence the work reported in this paper.

Acknowledgements

The authors are members of the Gruppo Nazionale Calcolo Scientifico-Istituto Nazionale di Alta Matematica (GNCS-INdAM) and were partially supported by INdAM, through GNCS research projects. This support is gratefully acknowledged.

References

[1] T.J. Hughes, J.A. Cottrell, Y. Bazilevs, Isogeometric analysis: CAD, finite elements, NURBS, exact geometry and mesh refinement, Comput. Methods Appl. Mech. Eng. 194 (2005) 4135–4195.
[2] J.A. Cottrell, T.J. Hughes, Y. Bazilevs, Isogeometric Analysis: Toward Integration of CAD and FEA, John Wiley & Sons, 2009.
[3] F. Auricchio, L.B.D. Veiga, T.J.R. Hughes, A. Reali, G. Sangalli, Isogeometric collocation methods, Math. Models Methods Appl. Sci. 20 (11) (2010) 2075–2107.
[4] F. Auricchio, L.B.D. Veiga, A. Reali, G. Sangalli, Isogeometric collocation for elastostatics and explicit dynamics, Comput. Methods Appl. Mech. Eng. 249 (2012) 2–14.
[5] D. Schillinger, J.A. Evans, A. Reali, M.A. Scott, T.J.R. Hughes, Isogeometric collocation: cost comparison with galerkin methods and extension to adaptive hierarchical NURBS discretizations, Comput. Methods Appl. Mech. Eng. 267 (2013) 170–232.
[6] C. Anitescu, Y. Jia, Y.J. Zhang, T. Rabczuk, An isogeometric collocation method using superconvergent points, Comput. Methods Appl. Mech. Eng. 284 (2015) 1073–1097.
[7] H. Lin, Y. Xiong, X. Wang, Q. Hu, J. Ren, Isogeometric least–squares collocation method with consistency and convergence analysis, J. Syst. Sci. Complex. 33 (5) (2020) 1656–1693.
[8] H. Lin, Q. Hu, Y. Xiong, Consistency and convergence properties of the isogeometric collocation method, Comput. Methods Appl. Mech. Eng. 267 (2013) 471–486.
[9] H. Lin, Y. Xiong, H. Hu, J. Yan, Q. Hu, The convergence rate and necessary-and-sufficient condition for the consistency of isogeometric collocation method, Appl. Math.-A J. Chin. Univ. 37 (2) (2022) 272–289.
[10] G. Li, H. Lin, Collocation and Mass Matrix in least–squares Isogeometric Analysis, Technical Report, arXiv preprint, 2025.
[11] L.D. Lorenzis, J.A. Evans, T.J.R. Hughes, A. Reali, Isogeometric collocation: Neumann boundary conditions and contact, Comput. Methods Appl. Mech. Eng. 284 (2015) 21–54.
[12] J.A. Evans, R.R. Hiemstra, T.J.R. Hughes, A. Reali, Explicit higher-order accurate isogeometric collocation methods for structural dynamics, Comput. Methods Appl. Mech. Eng. 338 (2018) 208–240.
[13] E. Marino, J. Kiendl, L.D. Lorenzis, Isogeometric collocation for implicit dynamics of three-dimensional beams undergoing finite motions, Comput. Methods Appl. Mech. Eng. 356 (2019) 548–570.
[14] H. Casquero, L. Liu, C. Bona-Casas, Y. Zhang, H. Gomez, A hybrid variational-collocation immersed method for fluid-structure interaction using unstructured T-splines, Int. J. Numer. Methods Eng. 105 (11) (2016) 855–880.
[15] M. Torre, S. Morganti, F.S. Pasqualini, A. Düster, A. Reali, Immersed isogeometric analysis based on a hybrid collocation/finite cell method, Comput. Methods Appl. Mech. Eng. 405 (2023) 115856.
[16] M. Torre, S. Morganti, A. Nitti, M.D.D. Tullio, F.S. Pasqualini, A. Reali, An efficient isogeometric collocation approach to cardiac electrophysiology, Comput. Methods Appl. Mech. Eng. 393 (2022) 114782.
[17] R.M. Aronson, J.A. Evans, Divergence-conforming isogeometric collocation methods for the incompressible Navier-Stokes equations, Comput. Methods Appl. Mech. Eng. 410 (2023) 115990.
[18] R.M. Aronson, J.A. Evans, Stabilized isogeometric collocation methods for hyperbolic conservation laws, Eng. Comput. 40 (6) (2024) 3451–3475.
[19] R.M. Aronson, C. Wetterer-Nelson, J.A. Evans, Stabilized isogeometric collocation methods for scalar transport and incompressible fluid flow, Comput. Methods Appl. Mech. Eng. 417 (2023) 116283.
[20] H. Gomez, L.D. Lorenzis, The variational collocation method, Comput. Methods Appl. Mech. Eng. 309 (2016) 152–181.
[21] M. Montardini, G. Sangalli, L. Tamellini, Optimal-order isogeometric collocation at Galerkin superconvergent points, Comput. Methods Appl. Mech. Eng. 316 (2017) 741–757.
[22] D. Wang, D. Qi, X. Li, Superconvergent isogeometric collocation method with greville points, Comput. Methods Appl. Mech. Eng. 377 (2021) 113689.
[23] D.E.D. Falco, E. Schiassi, F. Calabrò, Least Squares with Equality constraints Extreme Learning Machines for the resolution of PDEs, Technical Report, arXiv preprint, 2025.
[24] X. Zhang, X.-H. Liu, K.-Z. Song, M.-W. Lu, Least–squares collocation meshless method, Int. J. Numer. Methods Eng. 51 (9) (2001) 1089–1100.